Microsc. Microanal. 12, 327–330, 2006
DOI: 10.1017/S1431927606060430

Microscopy AND Microanalysis

Synthesis and Characterization of Doped and Undoped ZnO Nanostructures

Katie E. McBean,[1,*] Matthew R. Phillips,[1] and Ewa M. Goldys[2]

[1]*Microstructural Analysis Unit, University of Technology, Sydney, P.O. Box 123, Broadway NSW, 2007 Australia*
[2]*Division of Information and Communication Sciences, Macquarie University, North Ryde, 2109 Australia*

Abstract: Zinc oxide (ZnO) nanoparticles have been produced using precipitation methods from ethanolic solution. Rare-earth metal doping was performed, and the effect of lithium codoping on the luminescence properties of the rare-earth doped products was assessed. The resulting particles were characterized using cathodoluminescence and scanning electron microscopy. It was found that lithium significantly enhanced the cathodoluminescence signal from the rare-earth ions, which has been attributed to the increased integration of the rare-earth ions into the ZnO structure. The nanophase ZnO products were also annealed in argon, hydrogen, and oxygen, with hydrogen being the most successful for removing the broad defect emission present in as-grown samples and enhancing the ZnO near band edge emission.

Key words: zinc oxide, cathodoluminescence, rare-earth metal, doping, annealing

Introduction

In recent years, there has been a great deal of interest in the use of zinc oxide (ZnO) as a material for a wide range of applications. Of considerable interest are the light-absorbing and -emitting characteristics of this material, for use in applications such as phosphor technology, gas sensing (Li et al., 2004), lasers (Liu et al., 2004), pigments (Ekambaram, 2005), and sunscreens. There is also the desire to find new luminescent materials to use as biological labels (Chen & Gerion, 2005; Gupta & Gupta, 2005) for applications such as flow cytometry, medical imaging, and drug delivery. To be able to produce ZnO nanoparticles of a controlled size and luminescent properties, we must first understand how this material behaves and how that behavior changes when altering its chemistry and structure. This is achieved by characterizing many different samples in a variety of ways. In recent years, there have been numerous studies on the luminescence properties of undoped and doped ZnO (van Dijken et al., 2000; Wang et al., 2004; Alim et al., 2005; Shan et al., 2005) and, similarly, on the synthesis of this material (Zhang et al., 2002; Liu & Zeng, 2004; Wang et al., 2005). Despite this, the chemical origin of many of the luminescence peaks of ZnO remains highly controversial, and the role of charge compensating dopants on rare-earth incorporation is poorly understood at best.

Received May 12, 2005; accepted April 4, 2006.
*Corresponding author. E-mail: katie.mcbean@uts.edu.au

In this work, undoped and europium (Eu)-doped, terbium (Tb)-doped, and lithium (Li)-codoped ZnO nanoparticles have been synthesized. The resulting products were also annealed in different gaseous atmospheres, and the resulting products were then characterized using cathodoluminescence (CL) spectroscopy and scanning electron microscopy (SEM). Rare-earth metals were chosen as dopants because of their long-lived, spectrally narrow luminescence emissions in the visible range of the spectrum when in their trivalent form. Additionally, Li was used as a codopant to balance the trivalent charge of the rare-earth ions, which, if integrated into the ZnO structure, would occupy a Zn^{2+} vacancy. A codopant used in this capacity is commonly referred to as a charge compensator and should produce a more stable product.

Materials and Methods

The ZnO nanoparticles were synthesized by reacting equal volumes of an ethanolic zinc chloride solution (0.05 M) with an ethanolic solution of sodium hydroxide (0.20 M). This reaction was performed at room temperature, under constant stirring for 6 h. The resulting powders were harvested by centrifugation and washed in both MilliQ water and ethanol. Doped samples were prepared by stoichiometrically adding the relevant rare-earth salt (with an equivalent concentration of lithium chloride where noted) to the zinc solution before mixing.

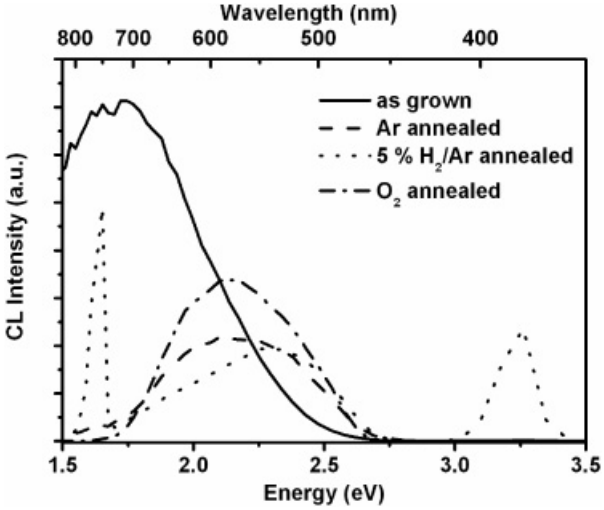

Figure 1. Cathodoluminescence spectra of undoped ZnO nanoparticles taken at 25 kV, 50 nA, 10 nm bandpass, 80 K, scan area 170 μm $\times$ 130 μm.

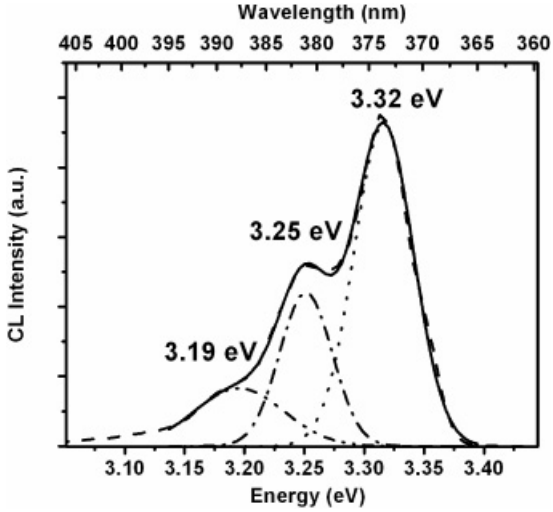

Figure 2. Near band edge emission from H_2-annealed ZnO nanoparticles showing LO phonon replicas with peak positions fitted as Gaussian curves; 25 kV, 50 nA, 1 nm bandpass, 80 K, scan area 170 μm $\times$ 130 μm.

Selected samples were annealed at 700°C for 10 min in atmospheres of either Ar, 5% H_2/Ar, or O_2. Annealing in Ar, an inert atmosphere, was used to observe the effect of the annealing process alone on the luminescence properties of the product. Conversely, 5% H_2/Ar and O_2 were used to observe the effects on the luminescence of the integration of hydrogen and oxygen, respectively, into the product. A 5% H_2/Ar mixture is used as a matter of safety and it is assumed that any observable differences between an Ar anneal and a 5% H_2/Ar anneal are due to the presence of hydrogen.

Cathodoluminescence spectra were collected using a JEOL 35C scanning electron microscope equipped with an Oxford Instruments MonoCL2 system, with a liquid nitrogen cold stage, and all were corrected for the system response. Secondary electron SEM images were obtained using a Zeiss Supra 55VP SEM using an in-lens detector.

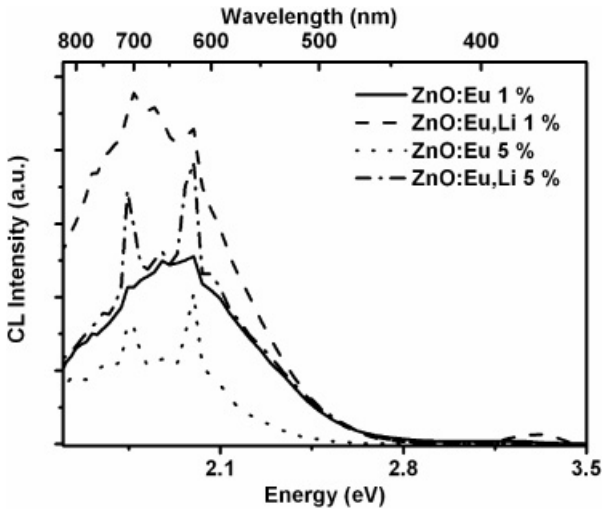

Figure 3. Cathodoluminescence spectra of Eu-doped, and Eu-Li-codoped ZnO nanoparticles; 25 kV, 50 nA, 10 nm bandpass, 80 K, scan area 170 μm $\times$ 130 μm.

Results

The CL spectrum of as-grown undoped ZnO nanoparticles (Fig. 1) has a very weak near band edge (NBE) emission at 3.3 eV (not visible at this scale) and a broad defect-related emission, made up of two peaks centered at 1.7 and 2.1 eV. After annealing in atmospheres of Ar and O_2, the emission centered at 1.7 eV is no longer present, whereas the emission at 2.1 eV remains and an additional emission, centered at 2.4 eV, is observed.

Annealing in an atmosphere of H_2, however, greatly enhances the NBE emission and quenches both the 1.7-eV and, to a lesser extent, 2.1-eV emissions. The sharp peak observed at 1.6 eV is the second-order emission arising from the NBE. The presence of longitudinal optical (LO) phonon replica peaks at ~70-meV intervals in the NBE emission (Fig. 2) indicate that postgrowth H_2 annealing produces a high-quality crystalline material.

Cathodoluminescence spectra of 1% and 5% Eu doped samples of ZnO, both with and without Li codoping, are shown in Figure 3. The 1% Eu doped samples display a broad defect emission, similar to the as-grown emission of undoped ZnO in Figure 1, and a very weak rare-earth emission at 2.0 eV. The 5% Eu doped samples, however, result in the appearance of an intense narrow emission from

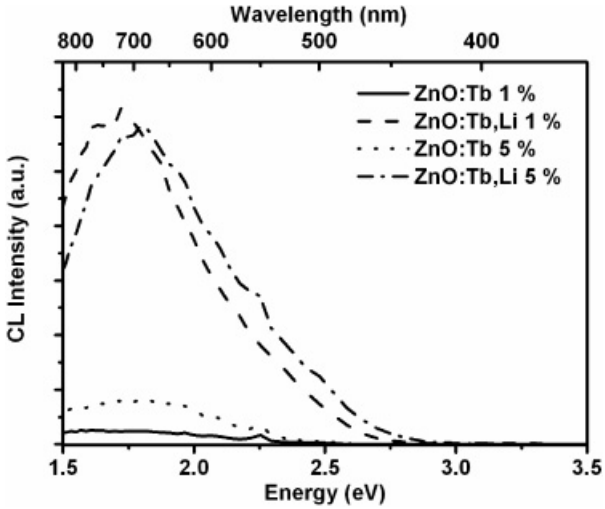

Figure 4. Cathodoluminescence spectra of Tb-doped and Tb-Li-codoped ZnO nanoparticles; 25 kV, 50 nA, 10 nm bandpass, 80 K, scan area 170 μm $\times$ 130 μm.

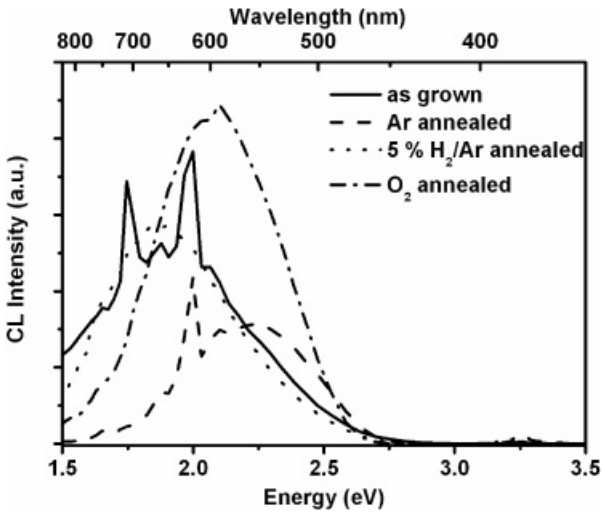

Figure 5. Cathodoluminescence spectra of ZnO:Eu, Li 5% nanoparticles; 25 kV, 50 nA, 10 nm bandpass, 80 K, scan area 170 μm $\times$ 130 μm.

Eu at 2.0 and 1.7 eV, assigned to the $^5D_0$-$^7F_2$ emission from Eu^{3+}.

The spectra from Tb doped ZnO are shown in Figure 4. Again, a broad defect emission is featured, attributed to the emissions at 1.7, 2.1, and 2.4 eV. Only a small peak is visible at 2.3 eV, where the most intense rare-earth emission line from the $^5D_4$-$^7F_5$ transition should appear.

The CL spectra in Figure 5 show that annealing in both H_2 and O_2 decreases the Eu emissions, whereas O_2 decreases the intensity of the emission at 1.7 eV while intensifying the emissions centered at 2.1 and 2.4 eV. Annealing in Ar decreases the intensity of all the CL peaks to some extent,

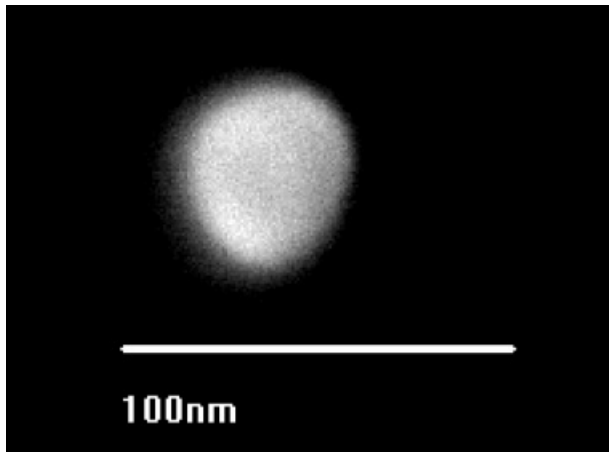

Figure 6. Secondary electron SEM image of a ZnO nanoparticle taken at 2 kV, with an in-lens detector.

although the rare-earth line at 2.0 eV is now more intense than the defect emissions.

SEM examination of the ZnO (Fig. 6) reveals the dimensions of the particles to be ~40 nm, although aggregation of smaller particles precluded obtaining precise measurements of their size.

Discussion

The annealing results for undoped ZnO (Fig. 1), clearly show that H_2 decreases the 1.7- and 2.1-eV defect emissions present in the as-grown ZnO and vastly enhances the NBE emission. It is the defect-related emission centered at 1.7 eV that is quenched by the annealing process, as its intensity was greatly reduced when annealed in all the gaseous atmospheres. The fact that the phonon replicas of the NBE emission (Fig. 2) can be seen shows that high-quality crystalline ZnO nanoparticles can be produced very easily by this wet chemical technique with the appropriate postprocessing.

The narrow emission from Eu^{3+} (Fig. 3) can only be detected when the initial concentration in solution is of the order of 5% of the Zn concentration. Codoping with Li appears to produce higher quality material with a smaller 1.7-eV defect emission. The Tb-doped ZnO, however, shows little evidence of any integration (Fig. 4), with only a very weak emission at 2.3 eV. Only the Tb–Li-codoped products exhibit an intense broad emission dominated by the 1.7-eV emission center, with a smaller contribution from the emission centered at 2.1 eV. This may indicate that some Tb^{3+} is incorporated on Zn^{2+} sites due to the presence of the charge-compensating Li^+ centers. The absence of the Tb^{3+} emission at 2.3 eV in these Li-codoped spectra may be due to the dominance of the defect emission. Additionally, the intense defect emission may result from Li integrated into

the ZnO producing more radiative recombination channels. The reason for this apparent lack of integration of Tb^{3+} into the ZnO, compared to Eu^{3+}, may be due to the large difference in the ionic radius of the Tb^{3+} (1.18 Å) to that of Zn^{2+} (0.74 Å). The radius of Eu^{3+} is slightly smaller (1.07 Å) and may, therefore, be accommodated more comfortably in the ZnO structure.

The spectra of ZnO:Eu, Li 5% after annealing (Fig. 5) differ somewhat from those for ZnO (Fig. 1). Here, the greatest decrease in intensity is observed for the 2.4-eV emission, and the rare-earth emission disappears entirely when annealed in O_2 and H_2. Annealing in Ar, however, results in a rare-earth emission of greater intensity than the defect emission.

Conclusions

It appears that annealing in H_2 is the most effective treatment, for both doped and undoped ZnO, to produce a stable product with the desired luminescence properties.

References

Alim, K.A., Fonoberov, V.A. & Balandin, A.A. (2005). Origin of the optical phonon frequency shifts in ZnO quantum dots. *Appl Phys Lett* **86**, 053103–053105.

Chen, F. & Gerion, D. (2005). Development of functionalized superparamagnetic iron oxide nanoparticles for interaction with human cancer cells. *Biomaterials* **26**, 2685–2694.

Ekambaram, S. (2005). Combustion synthesis and characterization of a new class of ZnO-based ceramic pigments. *J Alloy Comp* **390**, L4–L6.

Gupta, A.K. & Gupta, M. (2005). Synthesis and surface engineering of iron oxide nanoparticles for biomedical applications. *Biomaterials* **26**, 3995–4021.

Li, Q.H., Liang, Y.X., Wan, Q. & Wang, T.H. (2004). Oxygen sensing characteristics of individual ZnO nanowire transistors. *Appl Phys Lett* **85**, 6389–6391.

Liu, B. & Zeng, H.C. (2004). Room temperature solution synthesis of monodispersed single-crystalline ZnO nanorods and derived hierarchical nanostructures. *Langmuir* **20**, 4196–4204.

Liu, X., Yamilov, A., Wu, X., Zheng, J., Cao, H. & Chang, R.P.H. (2004). Effect of ZnO nanostructures on 2-dimensional random lasing properties. *Chem Mater* **16**, 5414–5419.

Shan, W., Walukiewicz, W., Ager, J.W., III, Yu, K.M., Yuan, H.B., Xin, H.P., Cantwell, G. & Song, J.J. (2005). Nature of room-temperature photoluminescence in ZnO. *Appl Phys Lett* **86**, 191911–191913.

van Dijken, A., Meulenkamp, E.A., Vanmaekelbergh, D. & Meijerink, A. (2000). Identification of the transition responsible for the visible emission in ZnO using quantum size effects. *J Lumin* **90**, 123–128.

Wang, J., Cao, J., Fang, B., Lu, P., Deng, S. & Wang, H. (2005). Synthesis and characterization of multipod, flower-like, and shuttle-like ZnO frameworks in ionic liquids. *Mater Lett* **59**, 1405–1408.

Wang, Q.P., Zhang, D.H., Xue, Z.Y. & Zhang, X.J. (2004). Mechanisms of green emission from ZnO films prepared by rf magnetron sputtering. *Opt Mater* **26**, 23–26.

Zhang, J., Sun, L., Yin, J., Su, H., Liao, C. & Yan, C. (2002). Control of ZnO morphology via a simple solution route. *Chem Mater* **14**, 4172–4177.